Evolution of the Surface Wind Field in an Intensifying Tropical Cyclone

JOHN MOLINARI AND STEVEN SKUBIS

Department of Atmospheric Science, State University of New York at Albany, Albany, NY 12222

(Manuscript received 19 February 1985, in final form 9 August 1985)

ABSTRACT

The surface wind field in a developing tropical cyclone (Agnes, 1972) was analyzed over a 1660 km radius for four days using conventional surface data, as the storm evolved from a disorganized depression to a hurricane. The transition to hurricane intensity was characterized by a wavelike disturbance propagating inward at 15 m s^{-1} from the outermost radii to the storm core over a 36-hour period. This propagating disturbance was clearly visible in the radial and vertical motion fields as a surge of inflow and upward motion. Rapid intensification of the storm began within hours after the leading edge of the surge reached the storm center. The analysis of consecutive 12-hour periods without compositing of data from nonsynoptic times was essential for identification of this feature.

The surge had the same asymmetry as the upper-level outflow channel, indicating the possible involvement of the outflow layer in its initiation. No clear evidence of an external forcing mechanism for the surge, such as the passage of an easterly wave across the circulation, could be found. No instability theory could account for propagation of this feature across regions with such strongly varying dynamical properties. As a result, it remains uncertain whether the inflow surge represented an environmental trigger to hurricane formation or a manifestation of an internal instability.

The boundary layer momentum budget was dominated by Coriolis torque and frictional dissipation. The sum of these two terms acted as a momentum source primarily during the passage of the inflow surge across each radial region. Inward lateral flux of momentum contributed significantly only within 440 km of the center.

A distinct diurnal oscillation in pressure tendency occurred until hurricane strength was reached, with maximum deepening at 1200 local time, and minimum deepening at 0000 local time. Diurnal oscillations in other variables were more subtle and often at variance with those described in other tropical cyclones.

Because the inflow surge developed at outer radii 36 hours prior to rapid deepening and had a clear signature in the time change of radial mass flux, it provides a potential tool for forecasting tropical cyclogenesis 24 hours or more in advance which requires only the use of conventional data. More study is needed to determine whether such an early warning signal frequently occurs in intensifying tropical cyclones.

1. Introduction

The nature of the process by which a tropical cyclone develops from a disorganized tropical depression remains inadequately understood, in large part because such intensification occurs over water, far from standard observation networks. The essential core structures of a hurricane, the eye and eye wall, make up a tiny fraction of the storm's circulation. Direct sensing of the development of this inner structure, which requires both massive resources (e.g., many instrumented aircraft at several levels) and knowledge of when (and where) to enter the incipient vortex, has not been achieved. Instead, our knowledge of the process of hurricane formation has largely evolved from observations on a scale larger than the inner region of the storm, and from theory and numerical modeling of idealized vortices.

Gray (1979) and McBride and Zehr (1981), using a large set of composited rawinsonde data, show distinct differences in the environments of developing and nondeveloping storms, particularly in lower- and upper-level vorticity. In the presence of intense convection, however, vorticity can be generated hundreds of kilometers from the convection within a few hours, especially in the outflow layer (e.g., Molinari and Corsetti, 1985). Because upper air data are collected only at 12-hour intervals, it is not clear whether the differences observed in developing and nondeveloping tropical disturbances precede or are a result of inner core intensification. Nevertheless, Gray (1979) describes one- to three-week fluctuations in the number of developing tropical disturbances, in the absence of fluctuation in the total number of disturbances, implying strong environmental control on the development process. Shapiro (1977) found that movement of a tropical wave into a region where nonlinear interactions with the wave are favored appears to be a necessary condition for development. Holland and Merrill (1984), using solutions to Eliassen's balanced vortex equation, suggest that upper level observed momentum forcing can directly influence events at the core of a developing storm. Because the above studies are diagnostic, neither they nor currently available observations can describe the time-dependent process by which environmental forcing interacts with the vortex.

In principle, numerical models can be used to address such a question. The majority of numerical studies form fairly realistic hurricanes with passive environments which allow exchange of momentum, heat, and moisture but contain no external asymmetric forcing. When asymmetries develop, they are the result of inertial instability in the outflow layer (e.g., Anthes, 1972). Holland and Merrill (1984), noting the rarity and probable transience of inertial instability, proposed that environmental forcing strongly regulates the intensification process, and that the mechanism of intensification in numerical models may be unrepresentative of that in nature, even though the final state is realistic.

Asymmetric environmental forcing has been incorporated in only a few numerical modeling studies. Tuleya and Kurihara (1981) examined the role of environmental shear on the initial development of an asymmetric vortex. Pfeffer and Challa (1981) showed that environmental interaction, in the form of parameterized inward eddy momentum flux in an axisymmetric model, accelerated development, and produced intensification at otherwise subcritical sea surface temperatures. In the above studies, the grid spacing was too coarse to resolve inner core dynamics, and cumulus parameterization enforced *a priori* a relationship between convection and the larger scale, which in reality is likely to vary as the intensification process proceeds (Rosenthal, 1978). As a result, environmental influences were incorporated, but the development of the inner core could not be explicitly addressed. Conversely, Willoughby *et al.* (1984a) describe the internal dynamics of the developing hurricane, including the eye and eye wall, with a detailed nonhydrostatic axisymmetric model, and obtain results quite similar to observations, without any asymmetry or environmental forcing. Due to limits in computer capacity and in the understanding of various microphysical processes in clouds, the next logical step, numerical modeling of the evolution of an asymmetric incipient vortex on a scale small enough to resolve inner core dynamics, yet over a region large enough to include an inhibiting or favorable environment, has yet to be attempted.

Three conclusions can be drawn: a) hurricanes can form in the absence of asymmetric environmental forcing, though such formation has not been observed; b) the hurricane environment influences the likelihood of intensification; and c) the relative importance of inner core dynamics and environmental forcing remains unclear, as does the process by which the environment influences events at the storm core.

The current study examines the wind field of an evolving vortex at the surface only, and thus cannot provide direct answers to the complex issues raised above. Indeed, both inner core dynamics (Ooyama, 1982) and environmental forcing (Gray, 1979) depend heavily on processes occurring above the surface layer. Nevertheless, by examining the time variation of the surface wind during a long period of evolution from depression to hurricane, this study will show fundamental changes in the behavior of the inflow layer, and will provide evidence for a relationship between an inflow surge beginning far from the storm center and subsequent intensity changes in the storm.

2. Synoptic overview

Surface wind fields were subjectively analyzed for seven observation times: 1200 GMT on 14 and 15 June 1972, and every 12 hours thereafter through 0000 GMT 18 June. (Hereafter, exact-hour observation times are expressed in a two digit format.) With the exception of two low-level cloud motion vectors and five aircraft reconnaissance reports (all on 00 GMT 16 June), the data were entirely conventional land and surface ship data, obtained from the Northern Hemisphere Data Tabulations (from the National Climatic Center) and U.S. Navy surface data (from the National Center for Atmospheric Research). Additional reports were taken from operational surface analyses obtained on microfilm from the National Hurricane Research Laboratory. Storm center positions were taken from aircraft reconnaissance reports (NOAA, 1972), linearly interpolated in time when necessary. During the first three observation times, prior to reconnaissance, center positions were determined subjectively from surface wind and pressure data and the operational analyses.

Analyses were tabulated on a cylindrical grid centered on the storm. Following common practice in hurricane studies, radial distances will be expressed in degrees latitude. The cylindrical grid has a radial increment of 1° latitude, an azimuthal increment of 15° and extends 15° latitude from the storm center. With a radial grid spacing of 111 km, the wind field inside of the one degree radius is essentially unknown. This study will not be concerned with the fine structure of the eye and eye wall, but of larger-scale influences on the development of the storm.

Only wind data taken at the observation time were used in each analysis. No attempt was made to incorporate data at intermediate times such as 06 or 18 GMT due to the presence of rapid changes in the circulation. Table 1 shows the mean station separation and its standard deviation in time for various radial regions, for the seven observation times studied. The station separation is given by

$$S = \left(\frac{\pi r^2}{N}\right)^{1/2},$$

where N is the number of observations within radius r. The small standard deviations indicate the relative uniformity of data density during the four-day period. The average area per observation represents 3 cylindrical grid points in the inner region and 1.7 grid points in the outer region. Thus, it is clear that local balances cannot be examined with the available data. Azimuthal means, however, which involve 24 grid points, will be

TABLE 1. Mean station separation for various radial regions and its standard deviation in time.

Radius increment (deg latitude)	Station separation (km)	Standard deviation (km)
0–2	204	20
0–6	230	31
0–10	244	23
0–14	261	19

shown to have coherent structure in space and time, and will be used to describe the evolution of the storm. The large scale of Agnes, which had azimuthal mean cyclonic flow and mean inflow out to the 15° radius for all times studied, even during the depression stage, helped to make this analysis possible. It is unlikely that a comparable data set would have been as useful during the earliest formative states on 11 and 12 June, when small-scale events may have been more dominant.

Figures 1a–g show the surface wind field of Agnes for each period and Fig. 2 shows the evolution of minimum central pressure, which was obtained from aircraft reconnaissance reports after 12 GMT 15 June, and from six-hourly analyses from the National Hurricane Center at prior times. Following the convention of Merrill (1984), the term "intensification" will refer to decreases in minimum central pressure or increases in inner region tangential wind, and "growth" will refer to an increase in circulation at middle or outer radii. The disturbance was already a tropical depression at the initial analysis time, with surface winds north of the center exceeding 10 m s^{-1}. The pressure field was weak and poorly organized until 18 GMT on 15 June, after which a 36-hour period of slow intensification began. The storm remained over land until between 00 and 10 GMT on 16 June, when it moved (or reformed) over water in the Yucatan Channel. At 16 GMT on 16 June, Agnes reached tropical storm strength. After a period of constant intensity, the central pressure fell rapidly starting between 06 and 12 GMT on 17 June, and Agnes reached hurricane strength at 22 GMT the same day as it moved east and then north through the Yucatan Channel. The clear asymmetry of the circulation, due in part to the large land mass to the west and southwest, was also visible on satellite pictures (Namias, 1973), which showed extensive cloud cover in the eastern quadrant, and almost none west and northwest of the center.

Subsequent to the final observation time in this study, Agnes moved north as a minimal hurricane and made landfall on the Florida peninsula at 22 GMT 19 June. Agnes later re-formed off the Atlantic coast and produced torrential rains and widespread flood damage in the middle Atlantic states. Dynamical processes acting during this latter stage are described by DiMego and Bosart (1982). In this study, the evolution of the surface radial and tangential winds and related quantities during the growth and intensification of Agnes will be described.

3. Development from depression to hurricane

a. Calculation method

Vertical motion at a level 50 mb above the surface was computed using

$$\omega = \int_{p_0-\Delta p}^{p_0} \left[\frac{1}{r}\frac{\partial}{\partial r}(ru) + \frac{1}{r}\frac{\partial v}{\partial \lambda}\right] dp, \qquad (2)$$

where u is radial velocity (positive outward), v tangential velocity (positive counterclockwise), and p_0 sea level pressure. For this computation as well as for momentum budget calculations (section 4), assumptions were required on the vertical variation of the wind in the lowest 50 mb. Initially the surface winds were assumed valid for the layer, following Riehl (1961), but momentum budget residuals showed a strong overestimate of $\partial M/\partial t$ due to unrealistically large Coriolis torque and lateral fluxes. In nature, the radial wind decreases fairly rapidly with height in the boundary layer (e.g., Jorgenson, 1984), while the overall wind speed changes by much less (e.g., Hawkins and Rubsam, 1968). The following two assumptions were made for all radii: a) the wind vector rotates 10° clockwise over the lowest 50 mb, following Frank (1977), whose composite tropical cyclone data showed this to be valid at least out to the 6° radius; and b) the total wind speed remains constant over the lowest 50 mb. These assumptions influenced only the momentum budget calculations and the magnitude of ω; all other variables were represented by their surface values obtained directly from the analyses. The sign of the azimuthal mean vertical motion ($\bar{\omega}$) was largely insensitive to the assumed rotation of the wind in the lowest 50 mb; a repeat calculation with a 50 percent increase in the veering angle to 15° did not change the sign of a single $\bar{\omega}$ value in the four-day period.

b. Evolution of storm structure

Figure 3 shows the rate of central pressure change in the storm computed after interpolating the values in Fig. 2 to three-hourly periods and using six-hour centered differencing in time. The distinct diurnal oscillation in $\partial p/\partial t$ will be discussed in section 4. A line connecting only 00 and 12 GMT values shows two periods of deepening, a slow deepening (4–5 mb day^{-1}) for 36 hours (12 GMT 15 June to 00 GMT 17 June), and a more rapid deepening to hurricane strength starting prior to 12 GMT 17 June and ending just after 00 GMT 18 June.

Tables 2–5 show radius-time sections of the azimuthal mean (hereafter simply "mean") values of tangential wind $\bar{v}$, radial wind $\bar{u}$, radial mass flux (represented by $\bar{u}r$), and vertical motion $\bar{\omega}$. A fundamental change in tangential velocity tendency occurred from

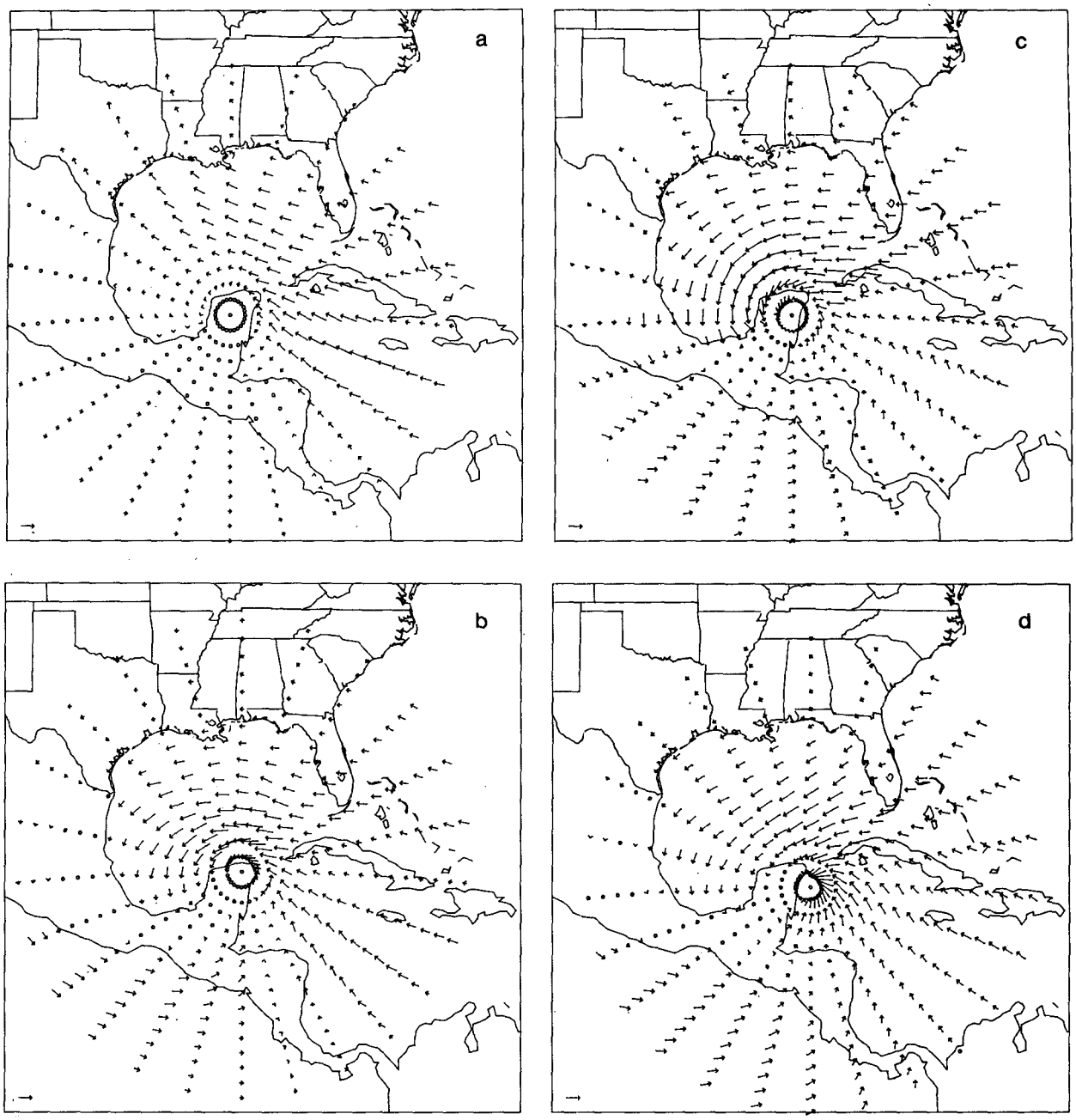

FIG. 1. Surface wind field for (a) 12 GMT 14 June; (b) 12 GMT 15 June; (c) 00 GMT 16 June; (d) 12 GMT 16 June; (e) 00 GMT 17 June; (f) 12 GMT 17 June; (g) 00 GMT 18 June. The vector at the lower left represents a speed of 10 m s^{-1}.

the depression to tropical storm and hurricane stages. During the first 36 hours, $\bar{v}$ increased at all middle and outer radii; the circulation grew in lateral extent but central pressure fell only slowly. Prior to tropical storm stage, tangential flow decreased from $r = 2°$ to 12°, and the subsequent intensification of Agnes occurred at progressively smaller radii, as outer and then middle radii decreased in strength of circulation.

Two radial-vertical circulations appeared to be active. The vortex-scale circulation, which can be crudely measured by the radius of maximum mean radial mass flux (at which $\bar{\omega}$ changes sign), grew to the outermost radius in the study by 12 GMT 16 June, then contracted to the 11° radius by 00 GMT 18 June (see Table 4). Superimposed upon this was an inner core circulation, located by a secondary maximum in mean radial mass flux, which appeared briefly at $r = 3°$ on 00 GMT 16 June (as indicated by subsidence outside

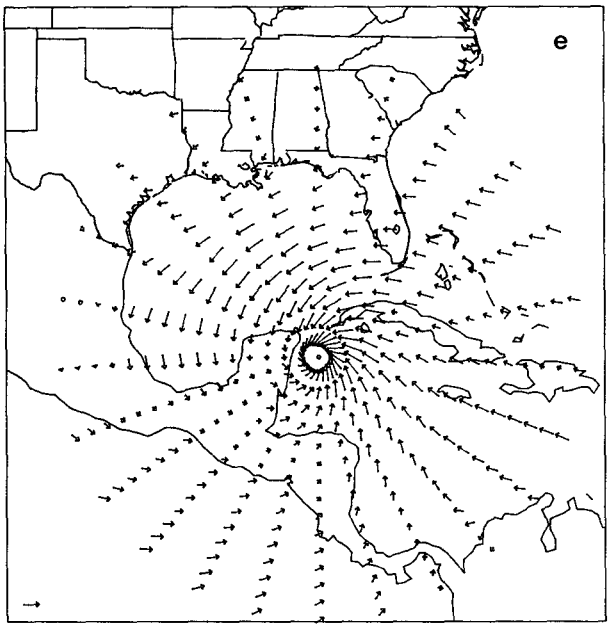

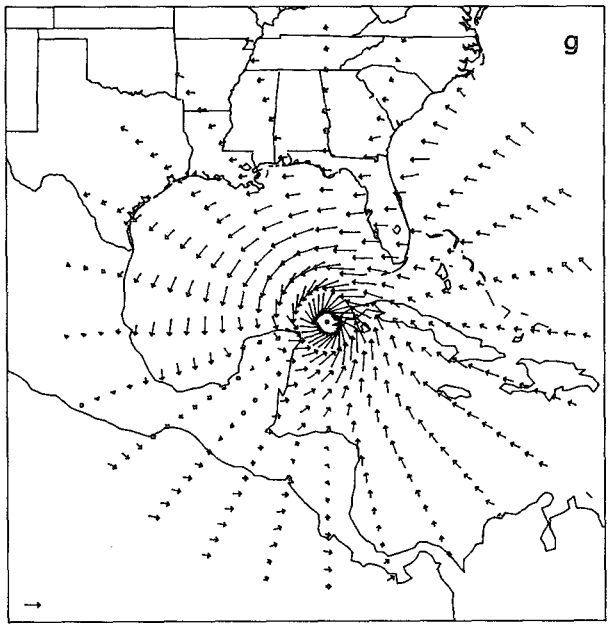

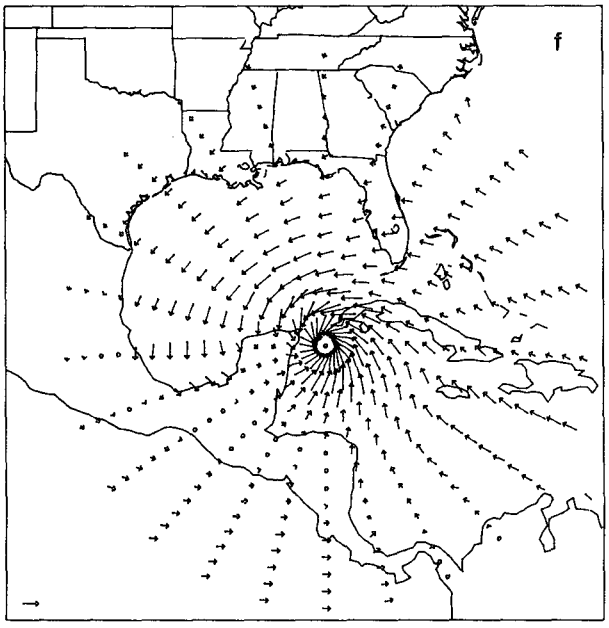

FIG. 1. (*Continued*)

the maximum), and reappeared at $r = 2°$ on 12 GMT 17 June through 00 GMT 18 June, when the storm reached hurricane strength. The mean transverse circulation on the vortex scale reached a maximum on 12 GMT 16 June, prior to tropical storm stage, and decreased thereafter while the inner region transverse circulation increased.

During the change in behavior at 12 GMT 16 June, the mean inflow increased at nearly all radii, and the maximum in inward mass flux (Table 4) shifted to 15°, the outermost radius in the study. At outer radii, the inflow reached its maximum in time (i.e., looking downward at a given radius in Table 3) at 12 GMT 16 June. These temporal inflow maxima, underlined at each radius in Table 3, shifted to middle radii by 00 GMT 17 June, and to inner radii by 12 GMT 17 June. The heavy solid line in Table 3 connects the positions of the geometrical center of this inflow surge at 12 GMT 16 June and 00 GMT 17 June; at $r = 9°$, the inflow was equal at the two observation times, and the center of the surge was assumed to reach that radius halfway between, at 18 GMT 16 June. The surge appears to

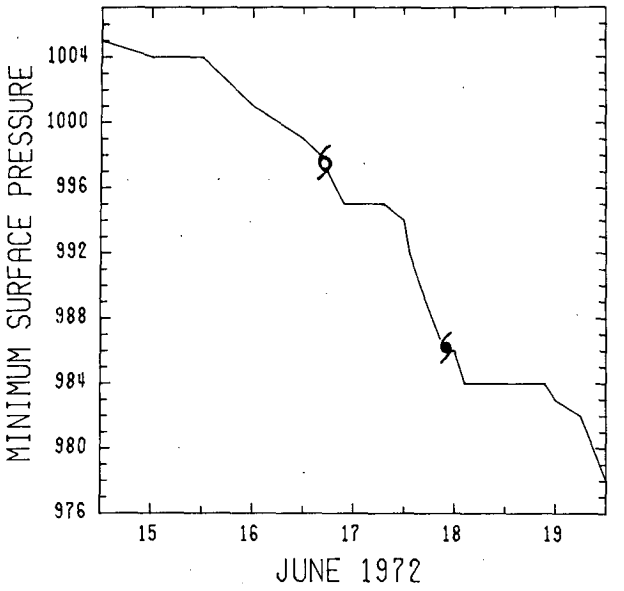

FIG. 2. Evolution of the minimum sea level pressure (mb) in the developing storm. Values were read from surface maps from the National Hurricane Center prior to 16 GMT 16 June, and from aircraft reconnaissance reports thereafter. Symbols indicate the times the storm reached tropical storm and hurricane intensity, respectively.

have propagated inward at a steady rate of about 15 m s^{-1}, and reached the center simultaneously (within the resolution of the data) with the beginning of the explosive deepening of the storm prior to 12 GMT 17 June.

Table 5 shows a region of increased upward motion at (and radially inward of) the mass flux maximum. This region appeared at the outermost radii at 00 GMT 16 June, propagated inward to middle radii over the subsequent 12 h, and to inner radii by 00 GMT 17 June. The explosive deepening did not begin when the vertical motion pulse first reached the inner regions of the storm, but instead several hours later, when the inflow was reaching its maximum. Given the large conditional instability outside the hurricane core (e.g., Frank, 1977), the regions of enhanced upward motion were likely to have been accompanied by pulses in convective heating. It is not possible with the given data to say whether a region of enhanced heating came first and generated the trailing inflow surge, or whether the acceleration in radial flow occurred first. The contraction of the vortex scale circulation as the surge propagated inward is shown in Table 5. Sinking motion appeared at the outermost radius at 00 GMT 17 June and shifted inward to the 10° radius 24 hours later as hurricane strength was attained.

Figure 4 shows the time variation of inward mass flux ($-\bar{u}r$) at selected radii. At $r = 12°$, mass flux grew steadily to a maximum at 12 GMT 16 June, then decreased as the surge passed. This maximum propagated toward the center with remarkable regularity 3° every six hours, which confirms the earlier phase speed estimate of 15 m s^{-1}. Because this propagating feature existed on a basic state which itself contained broad inflow, remaining figures will show 12-hour changes in mass flux in order to isolate the surge. Figure 5 shows the radial distribution of mass flux changes. A large convergence of radial mass flux associated with the surge appeared at outer radii at 00 GMT 16 June and produced the simultaneous increase in upward motion shown in Table 5. If the maximum at 00 GMT 16 June is assumed to have been located just outside the grid at $r = 16°$, its phase speed was 6° radius/12 h, identical to previous estimates. The loss of inward mass flux indicated in Fig. 5 as the wave propagated inward is likely due to conversion of radial to tangential momentum by Coriolis torque and by upward mass flux out of the boundary layer ahead of the strong flux convergence.

Figure 6 shows a radius–time section of 12-hourly mass flux changes. The heavy line represents $\Delta\bar{u}r = 0$ and thus the passage of the inflow maximum. Figure 6 shows the relatively large space and time scale of the surge and its dominance during the period of intensification. The largest changes in mass flux appear at outer radii, because mass flux is proportional to radius. A similar curve of $-\Delta\bar{u}$ (not shown) has the same zero line but shows maximum increases in inflow at inner radii just prior to rapid intensification.

The propagating wave has been shown only in azimuthal mean fields. In order to evaluate whether in fact it was a symmetric feature, the circulation was divided in half from southwest to northeast, based on

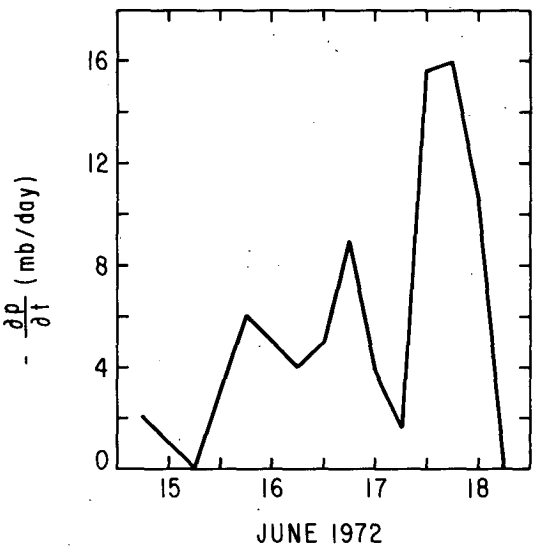

FIG. 3. Rate of change of minimum sea level pressure (mb/day), determined by interpolation of observed values from Fig. 2 to three-hour periods and six-hour centered differencing in time.

TABLE 2. Radius-time section of azimuthal mean tangential wind (m s^{-1}).

Day/time (June 1972)	Radius (degrees latitude)														
	1	2	3	4	5	6	7	8	9	10	11	12	13	14	15
14/12 GMT	0.0	1.3	2.6	2.7	3.0	3.0	3.1	2.6	2.2	1.6	1.1	1.2	1.2	1.1	1.1
15/12 GMT	3.6	5.7	5.8	5.9	5.3	4.6	4.4	3.9	3.1	2.3	2.2	2.2	2.3	2.3	2.5
16/00 GMT	1.7	5.6	6.7	6.9	6.6	6.2	5.7	5.7	5.4	4.9	4.1	3.5	3.0	3.0	2.9
16/12 GMT	3.2	3.9	4.5	4.9	5.2	5.3	4.7	4.2	4.3	3.9	3.5	3.3	3.2	3.4	3.5
17/00 GMT	5.5	5.3	5.6	5.7	5.7	6.1	5.9	5.5	5.0	4.4	3.9	3.0	2.9	2.8	3.0
17/12 GMT	7.3	9.4	8.0	6.8	6.1	5.6	5.0	4.4	4.1	3.7	3.5	3.0	2.9	2.9	2.8
18/00 GMT	8.0	10.8	10.3	7.9	7.0	6.4	5.4	4.4	4.1	3.7	3.5	3.0	2.9	3.0	3.0

satellite-observed cloud asymmetry, and twelve-hourly changes in net mass convergence for each half were plotted versus time for various semicircular annular regions. The mass convergence was computed using $-\oint v_n ds$, and thus includes azimuthal convergence of tangential velocity across the northeast and southwest parts of the circulation as well as the radial mass flux convergence, and is proportional to the area-averaged ω. Figures 7a, b show the changes in mass convergence for inner, middle, and outer regions for the southeast and northwest halves of the circulation. In the southeast half, the propagating wave showed distinctly and, as expected, had the same phase as the $\bar{\omega}$ propagation discussed earlier. In the northwest half, no evidence of a propagating feature was found. National Hurricane Center 200 mb maps, although containing sparse data, indicate an identical asymmetry in the outflow channel, which extended east and south for great distances, but not at all north and west, during the four-day period.

The observational aspects of the intensification of Agnes can be summarized as follows: a surge of inflow, preceded and accompanied by a band of upward motion, appeared more than 1660 km from the storm center, 36 h prior to rapid intensification. The surge, which was concentrated azimuthally in the half of the circulation containing the most cloudiness and under the upper level outflow channel, propagated steadily inward at a speed of 15 m s^{-1}. Within 12 h after the upward motion pulse reached the storm core, a period of rapid pressure falls commenced and the storm subsequently reached hurricane strength.

c. *Discussion*

During the early stages of the storm, when the center was diffuse and poorly organized, tangential circulation strengthened at outer radii. This growth in circulation undoubtedly created a more favorable environment for later intensification (Holland and Merrill, 1984). The maximum transverse circulation (measured by the radial mass flux) occurred prior to tropical storm stage, when the surge passed at outer radii. This vortex-scale circulation steadily decreased during subsequent intensification, and when hurricane strength was reached, outer region inward mass flux was weaker than during the disorganized depression stage at 12 GMT 15 June. These events support the finding of Gray (1979) that little correlation exists between the strength of the transverse circulation and storm intensity, and is consistent with Holland's (1983) observation that developing systems have weaker outer region transverse cir-

TABLE 3. Radius-time section of azimuthal mean radial wind (m s^{-1}). The largest inflow at each radius during the four-day period is underlined. The heavy solid line connects the geometrical center of these maxima at 12 GMT 16 June and 00 GMT 17 June.

Day/time (June 1972)	Radius (degrees latitude)														
	1	2	3	4	5	6	7	8	9	10	11	12	13	14	15
14/12 GMT	0.0	−0.6	−1.3	−1.3	−1.1	−1.2	−1.3	−1.5	−1.7	−1.6	−1.6	−1.4	−1.2	−1.0	−1.1
15/12 GMT	−0.9	−1.4	−1.2	−1.2	−1.1	−1.2	−1.7	−1.9	−2.1	−2.1	−1.9	−1.9	−1.7	−1.5	−1.2
16/00 GMT	−2.4	−3.7	−3.8	−3.0	−2.5	−2.4	−2.0	−2.1	−2.0	−2.0	−2.2	−2.2	−2.4	−2.4	−2.3
16/12 GMT	−5.3	−4.8	−3.9	−3.2	−2.9	−3.1	−3.0	−2.9	−3.2	−3.4	−3.4	−3.3	−3.3	−3.3	−3.1
17/00 GMT	−7.3	−7.0	−5.9	−4.9	−4.0	−3.9	−3.6	−3.3	−3.2	−3.1	−3.0	−2.8	−2.9	−2.7	−2.5
17/12 GMT	−13.0	−9.5	−6.4	−4.4	−3.3	−2.7	−2.4	−2.4	−2.4	−2.1	−2.0	−2.0	−2.0	−1.7	−1.7
18/00 GMT	−11.7	−8.3	−5.4	−3.7	−3.2	−2.9	−2.4	−2.3	−2.5	−2.2	−2.1	−1.8	−1.7	−1.5	−1.1

TABLE 4. Radius-time section of azimuthal mean radial mass flux $\bar{u}r$ (10^6 m^2 s^{-1}).

Day/time (June 1972)	Radius (degrees latitude)														
	1	2	3	4	5	6	7	8	9	10	11	12	13	14	15
14/12 GMT	0.0	−0.1	−0.4	−0.6	−0.6	−0.8	−1.1	−1.3	−1.7	−1.8	−2.0	−1.8	−1.7	−1.6	−1.8
15/12 GMT	−0.1	−0.3	−0.4	−0.5	−0.6	−0.8	−1.3	−1.6	−2.1	−2.3	−2.4	−2.5	−2.5	−2.3	−2.1
16/00 GMT	−0.3	−0.8	−1.3	−1.3	−1.4	−1.6	−1.6	−1.9	−2.1	−2.2	−2.6	−3.0	−3.5	−3.8	−3.8
16/12 GMT	−0.6	−1.1	−1.3	−1.4	−1.6	−2.1	−2.3	−2.6	−3.2	−3.8	−4.1	−4.4	−4.8	−5.1	−5.1
17/00 GMT	−0.8	−1.6	−2.0	−2.2	−2.2	−2.6	−2.8	−2.9	−3.2	−3.4	−3.7	−3.8	−4.1	−4.2	−4.2
17/12 GMT	−1.4	−2.1	−2.1	−1.9	−1.8	−1.8	−1.9	−2.1	−2.4	−2.4	−2.5	−2.6	−2.8	−2.7	−2.8
18/00 GMT	−1.3	−1.8	−1.8	−1.6	−1.8	−1.9	−1.9	−2.0	−2.5	−2.4	−2.6	−2.4	−2.4	−2.3	−1.9

culations than nondeveloping systems. The decrease in inner radii inflow during the period of most intense pressure falls after 12 GMT 17 June supports the findings of Schubert and Hack (1982). Thus, despite the presence of the surge, many aspects of the intensification of Agnes are consistent with previous observations and theory. Subsequent discussion will focus on the surge itself.

The surge is not visibly apparent in the raw data or the analyses, presumably because its amplitude outside the core, measured by 12 hourly radial velocity change, is less than 2 m s^{-1}. Because such a phenomenon has not previously been observed, it is necessary to rule out the possibility of analysis artifact. This issue can be addressed by examining Fig. 4. Considering first the curve for the 12° radius, each point is determined from entirely independent (i.e., nonoverlapping) data sets from different observation times, yet the time variation is exceptionally coherent, showing a rapid but steady rise to a peak, then a sharp fall. Using the mean station separation at outer radii given earlier, an average of 16 data points influence each value plotted on this line. A few spurious wind reports at a given hour, if they were erroneous enough to influence the azimuthal average, would produce a local spike in the graph, and none is apparent. For data or analysis errors to produce the evolution at $r = 12°$ over seven observation times would be highly unlikely. The remaining curves on Fig. 4 provide additional support for this view. Not only does the mean mass flux at each radius vary smoothly in time, but a systematic phase shift occurs across time periods. Given the roughly 230 km mean station separation, the analyses at $r = 6°$, for instance, are virtually independent of those at $r = 12°$. Thus it appears inconceivable that data or analysis errors could be present at the appropriate times and locations to produce the evolution shown. Although these arguments have been purely heuristic, we believe that the existence of an inward propagating wave on a scale large enough to simultaneously influence many observation points is the only possible interpretation of the data.

The timing of the surge suggests that it caused, directly or indirectly, the intensification of the storm to hurricane strength. As noted by Ooyama (1982), intensification cannot be attributed to frictional inflow in the surface layer alone, because intensification must occur first at midlevels to produce the increased inertial stability required to maintain the warm core (and surface pressure gradient) that drive the frictional inflow. The inflow surge in this study was apparently not frictionally forced, however, in that inflow decreased as the surge passed, even as the radial pressure gradient increased. It is conceivable that the enhanced inflow was directly related to the intensification through the process described by Ooyama (1982): enhanced inner core convection associated with the surge generated large midlevel "entrainment inflow" (Willoughby *et al.*, 1984a) into buoyant convective elements, which enhanced midlevel tangential flow and inertial stability

TABLE 5. Radius-time section of vertical motion (10^{-4} mb s^{-1}).

Day/time (June 1972)	Radius (degrees latitude)														
	0	1	2	3	4	5	6	7	8	9	10	11	12	13	14
14/12 GMT	0.0	−2.1	−3.4	−2.6	−0.6	−0.5	−1.3	−1.5	−1.7	−1.2	−0.8	0.0	0.6	0.4	−0.1
15/12 GMT	−4.9	−3.9	−1.6	−0.8	−0.7	−0.8	−2.1	−2.4	−2.1	−1.6	−0.6	−0.4	−0.1	0.3	0.7
16/00 GMT	−19.7	−14.5	−8.4	−2.1	0.2	−0.8	−0.5	−0.5	−0.9	−0.7	−1.2	−1.5	−1.6	−1.3	−0.3
16/12 GMT	−44.4	−20.1	−6.1	−1.7	−0.9	−2.0	−2.2	−1.4	−2.0	−2.6	−2.0	−1.2	−1.0	−0.9	−0.3
17/00 GMT	−61.0	−29.0	−10.6	−3.4	−0.7	−1.1	−1.5	−0.8	−0.9	−1.1	−1.0	−0.7	−0.8	−0.7	0.0
17/12 GMT	−110.0	−38.6	−5.4	1.7	2.0	0.9	−0.1	−1.0	−1.2	−0.5	−0.1	−0.5	−0.6	0.0	0.2
18/00 GMT	−98.0	−32.8	−2.7	2.0	0.4	−1.0	−0.4	−0.3	−1.7	−0.9	0.0	0.0	0.2	0.3	0.9

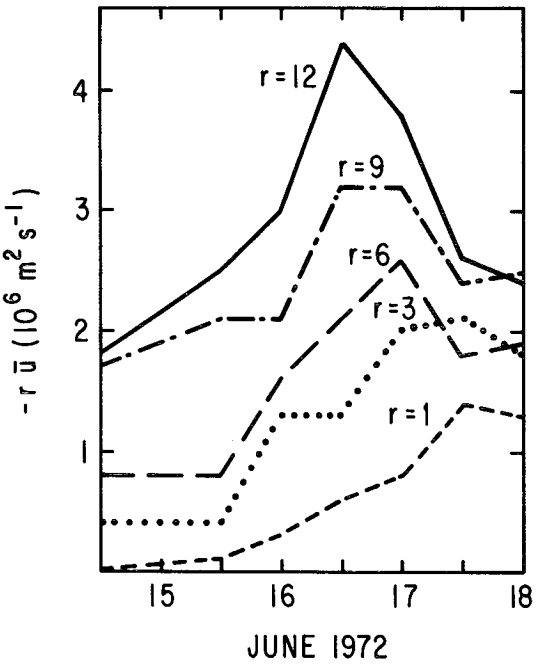

FIG. 4. Time variation of mean inward mass flux ($-\bar{u}r$) for selected radii.

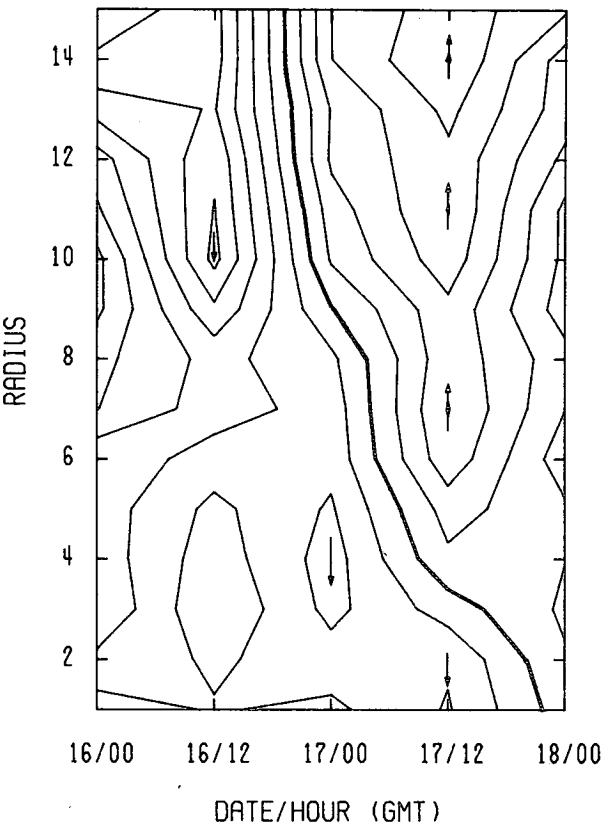

FIG. 6. Radius–time section of the change of inward mass flux for 12-hour periods ending at the hours shown. The heavy line, for which $\Delta\bar{u}r = 0$, represents the temporal maximum in inward mass flux at each radius. The contour interval is 3×10^5 m^2 s^{-1}.

and produced the core mass adjustments necessary to lower the surface pressure. The several hour lag between the enhanced vertical motion and the commencement of rapid intensification (see Fig. 3 and Table 5) is consistent with this view of the development of Agnes.

To the extent that the inflow surge brought about the subsequent intensification, two fundamental issues arise: the dynamics of inward propagation, in view of the usually observed outward motion of hurricane bands; and the initiation mechanism of the wave. The dynamics of inward contraction of a convective ring have been described by Shapiro and Willoughby (1982), and observations have confirmed that such an inward contraction frequently occurs in hurricanes, as an outer eye wall shifts inward and replaces the original eye wall (Willoughby *et al.*, 1982). The mechanism of this contraction requires a strong inward increase of inertial stability, which is not met at middle and outer radii, where inertial stability (not shown) is order f^2 and often increases outward. Because the surge originated at these radii, the mechanism of Shapiro and Willoughby (1982) is not a likely explanation for the inward propagation. Because the dynamical structure of the hurricane varies greatly from outer regions to the inner core where the Rossby number exceeds unity (e.g., Willoughby *et al.*, 1984b), the propagating surge may take on a different structure inside the 1° radius, and could conceivably represent a precursor to the formation of the outer eye wall observed by Willoughby

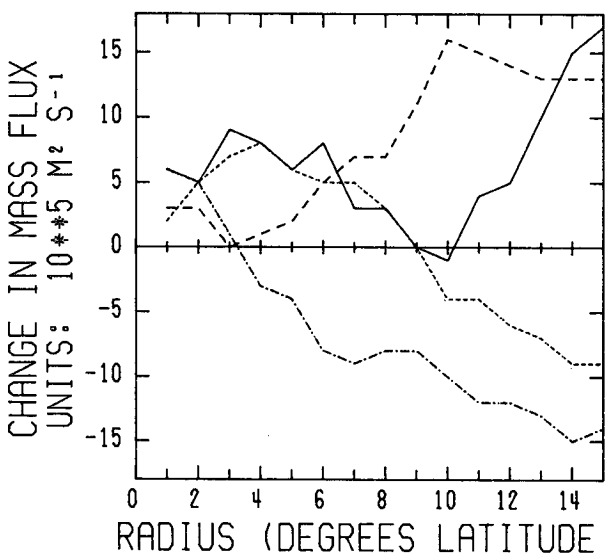

FIG. 5. Radial distribution of 12-hour changes in inward mass flux for the periods ending at 00 GMT 16 June (solid), 12 GMT 16 June (large dash), 00 GMT 17 June (small dash), and 12 GMT 17 June (dash–dot).

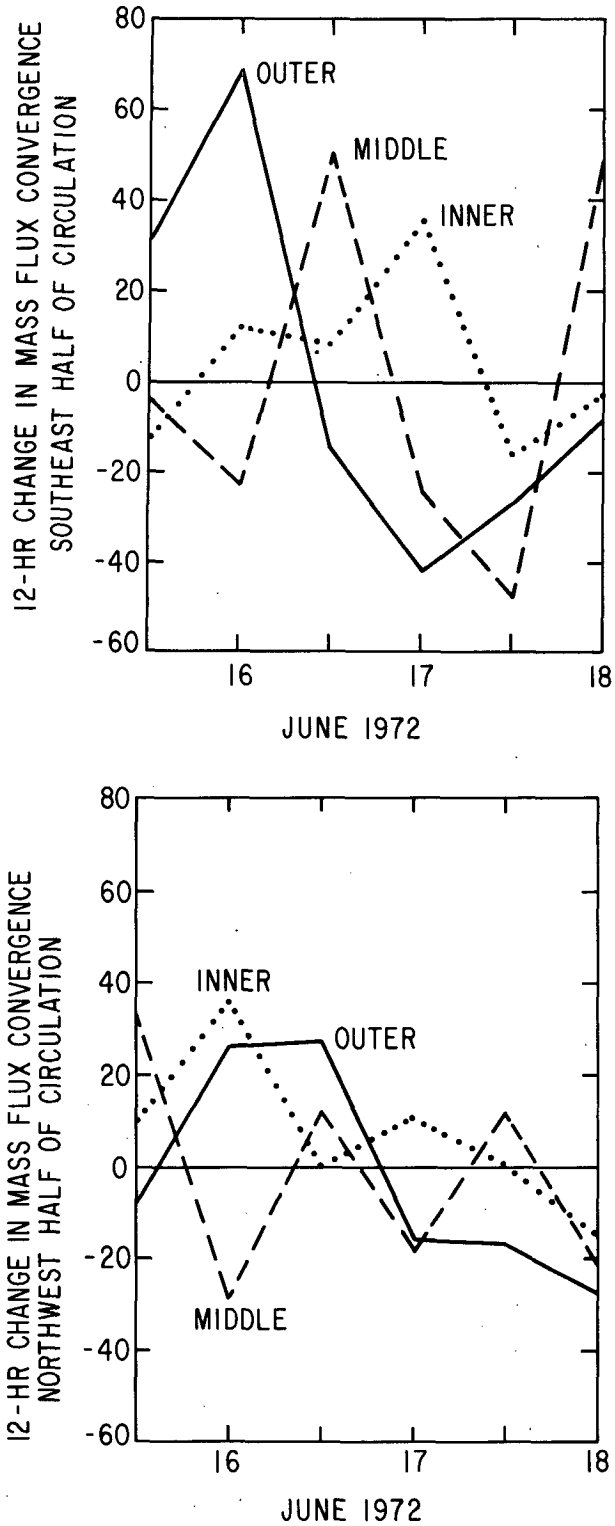

FIG. 7. Changes in net mass convergence ($-\Delta \oint v_n ds$) for the 12-hour period ending at the hours shown, for outer ($r = 9°$–$14°$; solid), middle (5°–9°; dashed), and inner (0°–4°; dotted) radii, averaged over (a) the southeast half of the circulation and (b) the northwest half.

et al. (1982). The mechanism of propagation outside the inner radii remains obscure.

The surge first appeared at the outermost radii in this study, and the question of its initiation mechanism cannot easily be addressed with the available data. In principle, the surge could represent a manifestation of an internal instability of the system. Anthes (1972) described the formation of bands of heating simultaneously with the occurrence of inertial instability in the outflow layer. His instability occurred much closer to the center than where the inflow surge started in Agnes, however, and limited 200 mb data in this case show no evidence of the presence of inertial instability, with maximum observed winds only 45 knots. Alternate mechanisms which could initiate rings of convection (Willoughby *et al.*, 1982) also are unlikely far from the center.

It appears more likely that some external forcing excited the wave. The feature was confined to the eastern part of the circulation and maintained a phase speed of 15 m s^{-1}, suggesting the possibility that an easterly wave moved across the region accompanied by a low-level surge of easterlies, and thus provided an external trigger to intensification of the system. Examination of all available soundings to the east at 850 and 700 mb, however, showed no evidence of the characteristic backing, then veering of the wind in time during easterly wave passage, and the origin of the surge remains uncertain.

Cause and effect is difficult to determine due to the cooperative nature of hurricane intensification and lack of data above the surface, but one clear statement of the order of events can be made: the inflow surge appeared first well outside of the center, propagated inward, and only subsequent to its reaching the center did rapid intensification occur. Circumstantial evidence suggests that the surge was associated in some manner with occurrences in the outflow layer. No instability theory in the literature indicates the presence of an inward propagating wave over such a great distance. It appears that a more complete set of observations or a time-dependent numerical integration would be required to determine the dynamics and initiation mechanism of this striking feature in Agnes.

4. Momentum budget

A momentum budget was constructed to investigate the important processes in the spinup of the surface layer. With the assumptions on vertical variation of the wind made earlier, the tangential and radial winds in the boundary layer can be written as

$$v(r, \lambda, p) = v_0(r, \lambda) \cos\left[\beta\left(\frac{p_0 - p}{\Delta p}\right)\right] - u_0(r, \lambda) \sin\left[\beta\left(\frac{p_0 - p}{\Delta p}\right)\right], \quad (3)$$

$$u(r, \lambda, p) = u_0(r, \lambda) \cos\left[\beta\left(\frac{p_0 - p}{\Delta p}\right)\right] + v_0(r, \lambda) \sin\left[\beta\left(\frac{p_0 - p}{\Delta p}\right)\right], \quad (4)$$

where $\beta = 10°$ is the assumed veering over the 50 mb layer and the subscript 0 indicates the surface value. The total relative angular momentum within radius r and depth Δp is

$$M = \frac{2\pi}{g} \int_{p_0 - \Delta p}^{p_0} \int_0^r \bar{m} r dr dp, \quad (5)$$

where the bar indicates an azimuthal average and $m = rv$. Using (3) and vertically integrating,

$$M = \frac{2\pi \Delta p}{g} \int_0^r r^2 \left[\frac{\sin\beta}{\beta} \bar{v}_0 - \left(\frac{1 - \cos\beta}{\beta}\right)\bar{u}_0\right] dr. \quad (6)$$

Following Anthes (1974) and Holland (1983), and using the vertical variation described above, the time rate of change of M can be written

$$\frac{\partial M}{\partial t} = -\frac{2\pi \Delta p}{g} \int_0^r r^2 \left[\frac{\sin\beta}{\beta} \overline{fu_0} + \frac{(1 - \cos\beta)}{\beta} \overline{fv_0}\right] dr - 2\pi \int_0^r r^2 [(\bar{\tau}_{z\lambda})_{p_0} - (\bar{\tau}_{z\lambda})_{p_0 - \Delta p}] dr - \frac{2\pi \Delta p}{g} r^2 \left[(\overline{v_0 u_0})_r \frac{\sin\beta \cos\beta}{\beta} + (\overline{v_0^2} - \overline{u_0^2})_r \frac{\sin^2\beta}{2\beta}\right] - \frac{2\pi}{g} \int_0^r r^2 [(\overline{v_0 \omega})_{p_0 - \Delta p} \cos\beta - (\overline{u_0 \omega})_{p_0 - \Delta p} \sin\beta] dr. \quad (7)$$

The terms represent, respectively, the conversion of radial to tangential momentum by Coriolis torque, frictional dissipation, lateral flux, and vertical flux. The instantaneous values of $\partial M/\partial t$ were computed for each radius and time using (7), and differences with observed values were sometimes large. Because $\partial M/\partial t$ in nature is much smaller than the two largest terms in the equation, the lack of agreement was not unexpected. The greatest uncertainty in (7) is contributed by frictional torque. To a first approximation, stress is largest at the surface and near zero ~100 mb above the surface, but its vertical variation in between is complex and dependent upon stability, wind speed, and other factors. The above problems were dealt with by adjusting the frictional torque to minimize the error between observed and calculated $\partial M/\partial t$. First, the difference in stress was written in terms of the surface stress alone:

$$(\bar{\tau}_{z\lambda})_{p_0} - (\bar{\tau}_{z\lambda})_{p_0 - \Delta p} = (\bar{\tau}_{z\lambda})_{p_0}(1 - K). \quad (8)$$

If stress were assumed to vary linearly from its surface value to zero in the lowest 100 mb, K would be 0.5. Equation (7) was calculated for several values, and $K = 0.3$ was found to minimize the mean absolute difference between observed and calculated $\partial M/\partial t$, equivalent to assuming that the stress profile is concave upward over the lowest 50 mb. The surface stress was evaluated from the quadratic stress law

$$(\tau_{z\lambda})_{p_0} = \rho_0 c_D |\mathbf{v}_0| v_0, \quad (9)$$

where $c_D = 5.2 \times 10^{-3}$ over land (Kung's (1968) geostrophic value multiplied by 0.6), and $c_D = 1.1 \times 10^{-3} + (4.5 \times 10^{-5})|\mathbf{v}_0|$ over water (Roll, 1965). Averaged over the seven observation times, the mean absolute error in $\partial M/\partial t$ was 20–30 percent of the Coriolis torque at all radii.

The assumptions made on vertical variation through the lowest 50 mb were designed to capture to first order the veering of the wind with height and evaluation of frictional torques via minimization of $\partial M/\partial t$. Although the procedures were somewhat crude, the error in $\partial M/\partial t$ was sharply reduced compared to assuming constant radial and tangential winds or linear variation of stress in the boundary layer.

Figures 8a–c show the time variation of the Coriolis torque for inner ($r = 0°$–$4°$), middle ($r = 4°$–$9°$), and outer ($r = 9°$–$14°$) regions of the circulation. The dominance of the inward propagating wave was apparent as a sharp peak shifted from outer to inner radii, corresponding to the surge in inflow seen in Fig. 4. Because Coriolis torque was always positive and one of the largest terms, the remaining terms in the momentum equation will be expressed as their ratio with the Coriolis torque.

Figures 9a–c show these ratios for friction, lateral flux, and vertical flux. At outer radii, dissipation of momentum by friction was generally less than generation by Coriolis torque, especially during the tropical depression stage and during the passage of the inflow surge. Lateral and vertical fluxes remained less than 20 percent of Coriolis torque at outer radii. Thus the outer region momentum balance was relatively simple: the circulation strengthened when conversion of inflow to tangential flow exceeded frictional dissipation, which occurred during early periods of weak inertial stability, and when the inflow surge passed.

At middle and inner radii, frictional dissipation more than consumed the momentum generated by Coriolis torque. The exceptions occurred during the passage of the inflow surge. Once tangential momentum was created by this process, dissipation, which is approximately proportional to v^2, quickly became dominant. Lateral and vertical fluxes tended to oppose each other. Their sum was a significant positive contribution at inner radii from 00 GMT 16 June onward. The anomalous values at 12 GMT 15 June at inner radii may reflect uncertainty in the storm center position, which was difficult to locate due to the poor organization of the surface pressure pattern at that hour.

The middle radii surface momentum budget can be

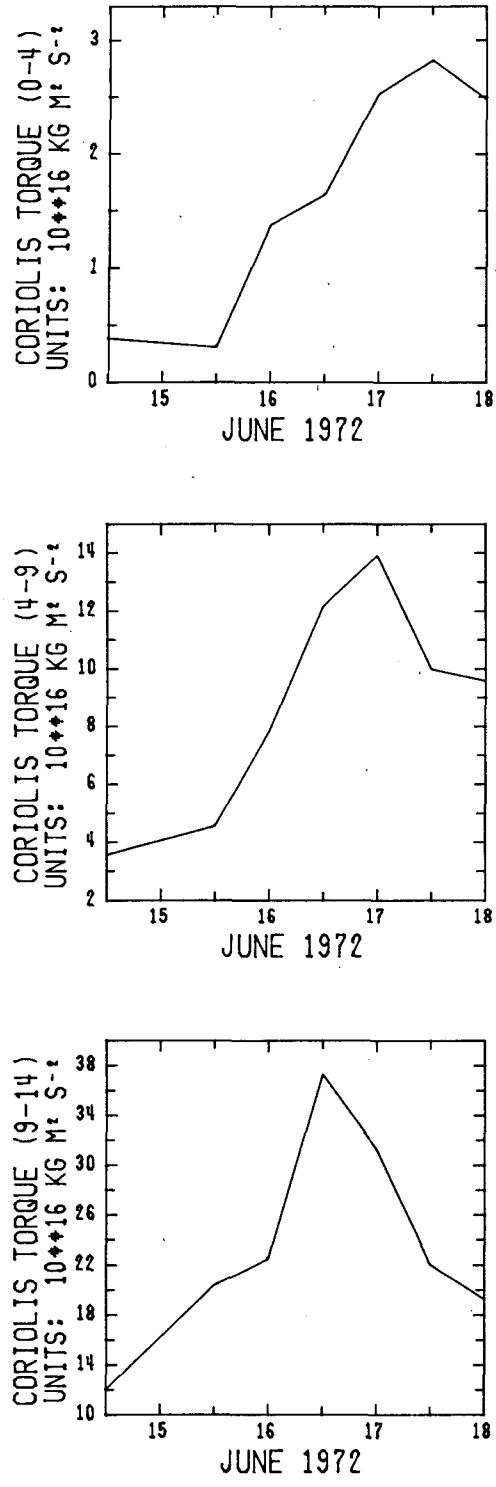

FIG. 8. Time change of total relative angular momentum contributed by Coriolis torque for (a) inner radii (r = 0°–4°); (b) middle radii (r = 4°–9°); and (c) outer radii (r = 9°–14°).

summarized as follows: friction consumed all the momentum generated by Coriolis torque, except during the passage of the inflow surge, and lateral flux convergence contributed only during early stages of development. At inner radii, Coriolis torque exceeded frictional dissipation only between the period when the storm first moved over water and the beginning of rapid intensification. Otherwise dissipation dominated, and the momentum supplied by the excess of lateral over vertical flux made an essential contribution to inner region intensification.

Overall, Coriolis torque and frictional dissipation dominated the boundary layer momentum budget,

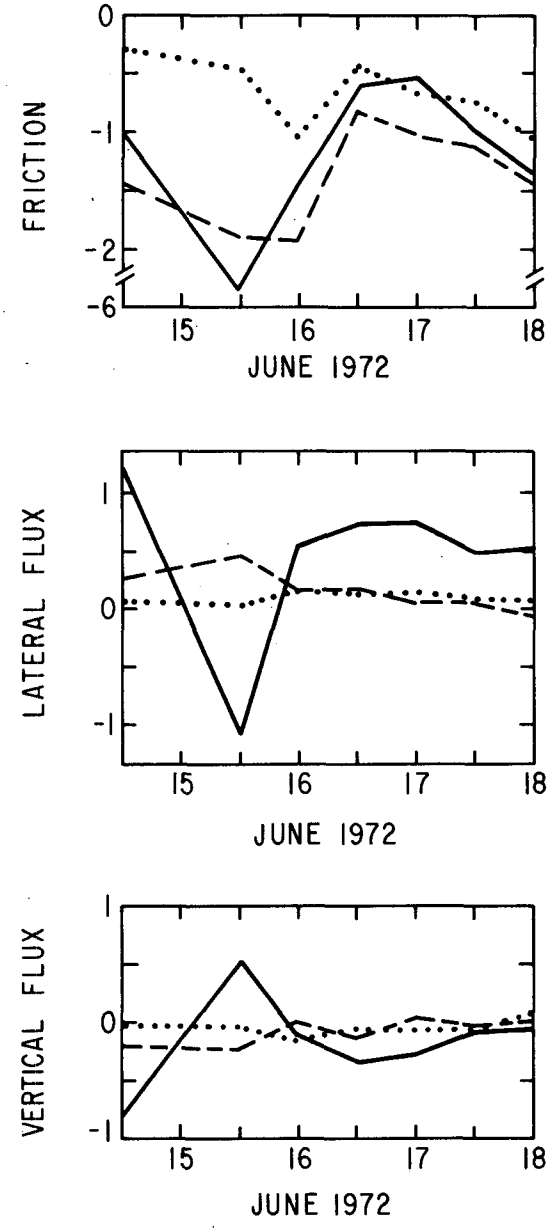

FIG. 9. Ratio of terms in the momentum equation to the Coriolis torque at each observation time for inner (solid), middle (dashed), and outer (dotted) radii for (a) frictional dissipation, (b) lateral flux and (c) vertical flux.

with lateral flux important only in the inner regions. The wave propagating inward across the circulation made a significant contribution as it passed.

5. Diurnal fluctuations

Diurnal fluctuations in tropical cyclones have been described in temperature and precipitation by Frank (1977), in vertical motion and divergence by McBride and Gray (1980), and in cloudiness by Muramatsu (1983) and Browner *et al.* (1977). Some contradictions exist in cloudiness variation for cloud top temperatures less than −50°C. Otherwise the following emerges: deep convection, vertical motion, and precipitation reach a diurnal maximum between 05 and 08 LST, and a minimum between 15 and 21 LST, within 3°–4° of the center. No oscillation in tangential wind, vorticity, or pressure has been identified.

The previous studies involve averages over many storms. The current study of only one storm has the advantage of not smoothing out significant features, at the possible expense of not being representative of all storms. Figure 3 shows a diurnal cycle in central pressure tendency which amplified over the four-day period, then vanished on 19 June (not shown) after hurricane strength was reached. The maximum rate of deepening each day was reached at 12 LST (18 GMT), and the minimum at 00 LST. This may be consistent with the 07 maximum in convective activity found in previous studies, in that the 4–6 hour lag may represent an adjustment time as enhanced entrainment inflow in the deep convection produces subsequent wind and mass adjustments as noted earlier. Frank (1977), using data available only at 10 and 22 LST, found evidence for this process being underway in a diurnal maximum in upper level temperatures at his earlier time.

Diurnal fluctuations in vertical velocity in this study are confounded by i) intensification of the storm; ii) presence of the inward propagating wave; and iii) the extensive land area near the storm, which has its own diurnal cycle. Figure 9c shows some evidence of a 19 LST (00 GMT) maximum in upward motion at inner radii, and an 07 LST maximum at middle radii, but with so many processes acting simultaneously, no clear signal stands out.

Somewhat surprisingly, a distinct diurnal oscillation was present in tangential velocity at middle radii, but not at inner radii, where it may have been masked by intensity changes, nor at outer radii. Figure 10 shows that, in part, this oscillation occurred over land, and was likely related to the decoupling of the surface layer from the large-scale pressure gradient over land at 12 GMT (07 LST). Nevertheless, an oscillation remained in $\bar{v}$ over water, with minimum speed at 07 LST, which is consistent with the diurnal pressure tendency shown in Fig. 3. No other diurnal oscillation was found. It is possible that other oscillations were present that could not be seen in the twice daily analyses.

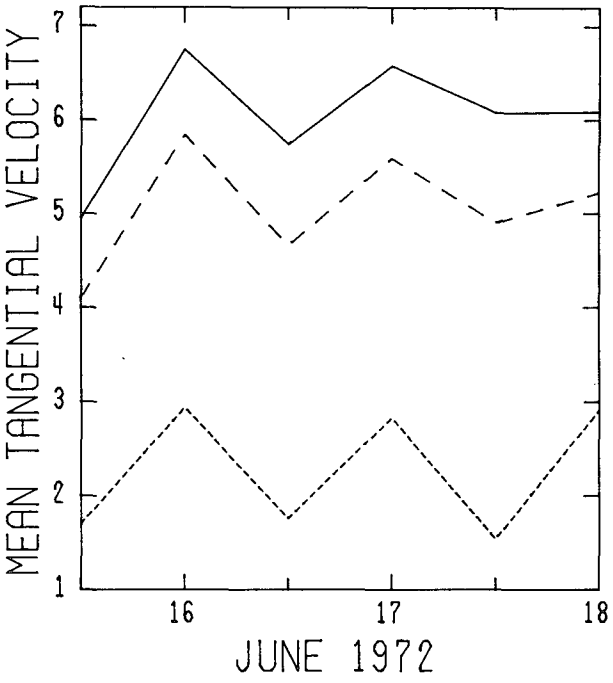

FIG. 10. Diurnal variation for middle radii (r = 5°–9°) of mean tangential wind over water (solid) and over land (small dash), and of the azimuthal mean tangential wind (large dash), which is the area-weighted average of the two.

6. Summary and conclusions

The evolution of the surface layer of a developing tropical cyclone was investigated over an 84-hour period. During the depression stage, the circulation strengthened over a broad region extending beyond the 1660 km radius, while the storm core remained disorganized and over land. During the final stages of development to hurricane strength, an inner circulation intensified while middle and outer circulations weakened. The transition between these regimes was dominated by a wavelike disturbance propagating inward at 15 m s^{-1} from the outermost radii to the storm center over a 36-hour period. This propagating feature, visible in the radial and vertical motion fields as a surge of inflow and upward motion, played a prominent role in generation of angular momentum at all radii as it passed, and rapid intensification began shortly after it reached the storm core. The propagation was not symmetric, but existed only in the southeastern half of the circulation, in the region occupied by the outflow channel at upper levels. The intensification appears to have followed the process described by Ooyama (1982): the sharp increase in convective heating at the storm core excited by the vertical motion pulse produced increased entrainment inflow into buoyant cloud elements at midlevels, and the adiabatic response to the subsequent midlevel spinup resulted in warming of the core and an increase in the low-level radial pressure

gradient. The fundamental questions of the initiation mechanism and dynamics of propagation of the wave could not be determined from the data set, but it clearly had its beginnings outside the 1660 km radius, and clearly preceded rapid intensification of the storm.

Because the existence of an inward propagating wave starting far from the center of developing tropical cyclones has not previously been described, it is conceivable that this feature is unique to Agnes, and that many alternate modes of environmental interaction and inner core intensification occur in nature. To the authors' knowledge, however, no previous study has examined the evolution of a storm over several consecutive periods without composited data. The variations shown in Figs. 4–7 indicate that propagation might have been entirely missed had the data been composited over 24-hour periods. One goal of future work must be to establish whether a propagating inflow surge frequently accompanies tropical cyclogenesis. For study of more recent storms than Agnes, this task should be aided by the availability of satellite-derived low cloud motion vectors (e.g., Rodgers and Gentry, 1983), the possibility of remotely sensed surface winds (Maresca and Barnum, 1979), and the use of omega dropwindsondes (ODW; Burpee *et al.*, 1984). The ODW data may also provide a measure of the vertical structure of radial flow and its time variation, which may shed more light on the dynamical processes involved in the propagation.

Thermodynamic and moisture fields were not examined in this study. Agnes formed over anomalously warm water (Namias, 1973), and it has been implicitly assumed that air reaching the center contained sufficient energy to rise to high levels in the troposphere. A moisture budget analysis may provide additional insight into the development process.

The inflow surge may represent an external trigger to tropical cyclone intensification, or may be a manifestation of some internal instability. The external trigger most supported by the propagation characteristics, the passage of an easterly wave across the circulation, was not supported by time series of the few rawinsonde stations to the east. The internal mechanism of outflow layer inertial instability also was not supported by the limited data available. Although it has been posed in a different manner, the question of the relative importance of environmental forcing and inner core dynamics remains.

Regardless of its initiation mechanism, the propagating wave provides a potential tool for forecasters. The surge appeared at outer radii 36 hours prior to rapid intensification, and had a distinct signature in the radial mass flux (see Figs. 4–7) as it propagated inward. If such a feature commonly occurs, it should be possible to identify it in real time, and tropical cyclogenesis might be predictable a full day or more in advance with only the use of conventional data.

Acknowledgments. The authors benefited from discussion with Hugh Willoughby of the Hurricane Research Division (HRD) of AOML/NOAA. Peter Black, also of HRD/AOML/NOAA, suggested the possibility of easterly wave passage triggering the surge. This research is supported by National Science Foundation Grant ATM-8317104.

REFERENCES

Anthes, R. A., 1972: Development of asymmetries in a three-dimensional numerical model of the tropical cyclone. *Mon. Wea. Rev.*, **100,** 461–476.

——, 1974: The dynamics and energetics of mature tropical cyclones. *Rev. Geophys. Space Phys.*, **12,** 495–522.

Browner, S. P., W. Woodley and C. Griffith, 1977: Diurnal oscillation of the area of cloudiness associated with tropical storms. *Mon. Wea. Rev.*, **105,** 856–864.

Burpee, R. W., D. G. Marks and R. T. Merrill, 1984: An assessment of omega dropwindsonde data in track forecasts of Hurricane Debby (1982). *Bull. Amer. Meteor. Soc.*, **65,** 1050–1058.

DiMego, G. J., and L. F. Bosart, 1982: The transformation of tropical storm Agnes into an extratropical cyclone. Part II: Moisture, vorticity, and kinetic energy budgets. *Mon. Wea. Rev.*, **110,** 412–433.

Frank, W. M., 1977: The structure and energetics of the tropical cyclone I. Storm structure. *Mon. Wea. Rev.*, **105,** 1119–1135.

Gray, W. M., 1979: Hurricanes: Their formation, structure, and likely role in the tropical circulation. *Meteorology Over the Tropical Oceans,* D. B. Shaw, Ed., *Roy. Meteor. Soc.*, 155–218.

Hawkins, H. F., and D. T. Rubsam, 1968: Hurricane Hilda, 1964. II. Structure and budgets of the hurricane on 1 October 1964. *Mon. Wea. Rev.*, **96,** 617–636.

Holland, G. J., 1983: Angular momentum transports in tropical cyclones. *Quart. J. Roy. Meteor. Soc.*, **109,** 187–210.

——, and R. T. Merrill, 1984: On the dynamics of tropical cyclone structural changes. *Quart. J. Roy. Meteor. Soc.*, **110,** 723–745.

Jorgenson, D. P., 1984: Mesoscale and convective-scale characteristics of mature hurricanes: Part II: Inner core structure of Hurricane Allen (1980). *J. Atmos. Sci.*, **41,** 1287–1311.

Kung, E. C., 1968: On the momentum exchange between the atmosphere and earth over the Northern Hemisphere. *Mon. Wea. Rev.*, **96,** 337–341.

Maresca, J. W., Jr., and J. B. Barnum, 1979: Remote measurement of the position and surface circulation of Hurricane Eloise by HF skywave radar. *Mon. Wea. Rev.*, **107,** 1648–1652.

McBride, J. L., and W. M. Gray, 1980: Mass divergence in tropical weather systems. Paper I. Diurnal variation. *Quart. J. Roy. Meteor. Soc.*, **106,** 501–516.

——, and R. Zehr, 1981: Observational analysis of tropical cyclone formation. Part II: Comparison of nondeveloping versus developing systems. *J. Atmos. Sci.*, **38,** 1132–1151.

Merrill, R. T., 1984: A comparison of large and small tropical cyclones. *Mon. Wea. Rev.*, **112,** 1408–1418.

Molinari, J., and T. Corsetti, 1985: Incorporation of cloud-scale and mesoscale downdrafts into a cumulus parameterization: Results of one and three-dimensional integrations. *Mon. Wea. Rev.*, **113,** 485–501.

Muramatsu, T., 1983: Diurnal variations of satellite-measured T_{BB} areal distribution and eye diameter of mature typhoons. *J. Meteor. Soc. Japan,* **61,** 77–90.

Namias, J., 1973: Birth of Hurricane Agnes—Triggered by the trans-equatorial movement of a meso-scale system into a favorable large-scale environment. *Mon. Wea. Rev.*, **101,** 177–179.

NOAA (National Oceanic and Atmospheric Administration), 1972:

Hurricane Agnes, Office of Meteorological Operations, Silver Spring, MD, 193 pp.

Ooyama, K. V., 1982: Conceptual evolution of the theory and modeling of the tropical cyclone. *J. Meteor. Soc. Japan,* **60,** 369–379.

Pfeffer, R. L., and M. Challa, 1981: A numerical study of the role of eddy fluxes of momentum in the development of Atlantic hurricanes. *J. Atmos. Sci.,* **38,** 2393–2398.

Riehl, H., 1961: On the mechanisms of angular momentum transport in hurricanes. *J. Meteor.,* **18,** 113–115.

Rodgers, E., and R. C. Gentry, 1983: Monitoring tropical-cyclone intensity using environmental wind fields derived from short-interval satellite images. *Mon. Wea. Rev.,* **111,** 979–996.

Roll, H. V., 1965: *Physics of the Marine Atmosphere.* Academic Press, 426 pp.

Rosenthal, S. L., 1978: Numerical simulation of tropical cyclone development with latent heat release by the resolvable scales I: Model description and preliminary results. *J. Atmos. Sci.,* **35,** 258–271.

Schubert, W. H., and J. J. Hack, 1982: Inertial stability and tropical cyclone development. *J. Atmos. Sci.,* **39,** 1687–1697.

Shapiro, L. J., 1977: Tropical storm formation from easterly waves: a criterion for development. *J. Atmos. Sci.,* **34,** 1007–1021.

——, and H. E. Willoughby, 1982: The response of balanced hurricanes to local sources of heat and momentum. *J. Atmos. Sci.,* **39,** 378–394.

Tuleya, R. E., and Y. Kurihara, 1981: A numerical study on the effects of environmental flow on tropical storm genesis. *Mon. Wea. Rev.,* **109,** 2487–2506.

Willoughby, H. E., J. A. Clos and M. G. Shoreibah, 1982: Concentric eye walls, secondary wind maxima, and the evolution of a hurricane. *J. Atmos. Sci.,* **39,** 395–411.

——, H.-L. Jin, S. J. Lord and J. M. Piotrowicz, 1984a: Hurricane structure and evolution as simulated by an axisymmetric, nonhydrostatic numerical model. *J. Atmos. Sci.,* **41,** 1169–1186.

——, F. D. Marks, Jr. and R. J. Feinberg, 1984b: Stationary and moving convective bands in hurricanes. *J. Atmos. Sci.,* **41,** 3189–3211.